The Free Internet Journal for Organic Chemistry

Paper

Archive for Organic Chemistry

Arkivoc **2017**, part v, 268-292

Development of a Karplus equation for $^3J_{COCH}$ in ester-functionalized glucopyranoses and methylglucuronate

Sven Hackbusch, Amelia Watson, and Andreas H. Franz*

Department of Chemistry, University of the Pacific, 3601 Pacific Avenue, Stockton, CA 95211, USA
Email: afranz@pacific.edu

Received 03-24-2017 **Accepted** 07-27-2017 **Published on line** 11-19-2017

Abstract

Empirical Karplus equations are very useful in the conformational analysis of flexible molecules, especially with regards to carbohydrates. The C(sp^2)OCH dihedral angle of ester-functionalized carbohydrates, however, is not well described by widely used Karplus equations for COCH dihedral angles, because they are based on C(sp^3)OCH data. Herein, we propose a three parameter Karplus equation of the form $^3J_{COCH}$ = 5.18 cos^2(θ*) – 1.42 cos(θ*) + 1.05 on the basis of quantum mechanics computations for 6-*O*-acetyl-α/β-D-glucopyranose. The equation gives satisfactory agreement between experimentally determined $^3J_{CH}$ values and those back calculated from MD simulations using the GLYCAM06 forcefield for a set of acetylated glucoses and methyl glucuronate.

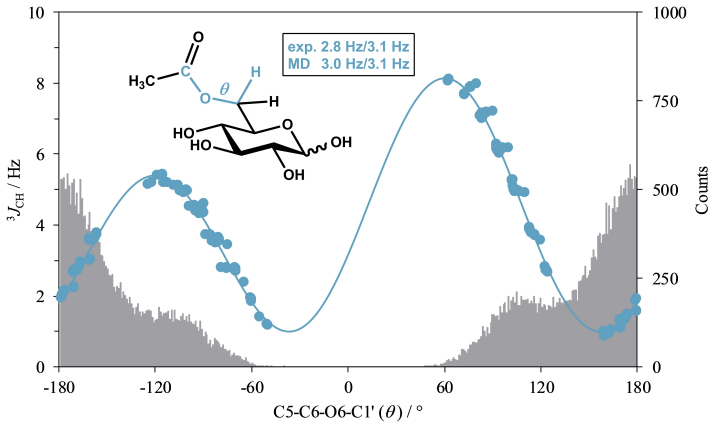

Keywords: NMR, Karplus equation, conformational analysis, molecular dynamics, carbohydrates, ester linkage

Introduction

Carbohydrates are inherently flexible molecules and attempts to shed light on the relation between structure and biochemical function of carbohydrates and their derivatives must be based on unambiguous structure assignment and the description of their solution geometries, otherwise known as Conformational Analysis. NMR spectroscopy, taken in conjunction with computational techniques and fitting procedures, can provide a near-complete picture of a molecule's solution geometry.[1-5] A particularly useful tool to determine a molecule's geometry is the Karplus relation between a coupling constant and dihedral angle of the coupled atoms, based originally on the Fermi Contact contribution in the early theories of NMR coupling phenomena.[6-8] The Karplus equation can describe quantitatively the correlation of experimental coupling constant to the dihedral angle between the coupled nuclei and has been used very successfully to derive molecular structures. Nowadays, such equations are based on a multitude of experimental data and extensive quantum mechanical calculations, which take bond lengths, electron densities, electron orbital terms, and dipolar electron spin terms into account.[9-12]

In our research efforts to investigate the conformational changes imparted by an ester linkage to novel ester-linked disaccharides, we required an accurate description of the flexibility of the C(sp^2)-O-C-H torsional angle to more accurately describe the solution state structure of these molecules. Many Karplus equations have been derived based on both experimental and computational data for HCCH, CCCH and COCH torsions, both for generalized and carbohydrate-specific cases.[10,13] However, as became evident based on preliminary work (as detailed in the Supplemental Material), the available Karplus equations for C(sp^3)OCH torsions were not well suited for ester-linked compounds due to the different hybridization of the carbonyl carbon. Specifically, the Karplus equations yield lower absolute values for the coupling in the sp^3-hybridized case compared to C(sp^2)-O-C-H in ester-functionalized compounds. Another publication by González-Outeiriño *et al.*, based on crystal structure data of acetate compounds, yielded a similarly disparate equation.[14] Thus, we decided to establish the Karplus relationship between the $^3J_{Csp2\text{-O-C-H}}$ coupling constants and the corresponding torsion angle θ (defined as C5-C6-O6-C1' based on IUPAC nomenclature, Figure 1) based on experimental and computational data for a model carbohydrate derivative, namely 6-*O*acetyl-*α/ß*-D-glucopyranose **1**. In addition, four more compounds were synthesized in acetyl 6- *O*acetyl-*α/ß*-D-glucopyranoside **2,** 2,6-di-*O*-acetyl-*α/ß*-D-glucopyranose **3**, 3,6-di-*O*acetyl-*α/ß*-D-glucopyranose **4** and methyl α/ß-D-glucopyranuronate **5** to serve as the test set to validate the Karplus equation.

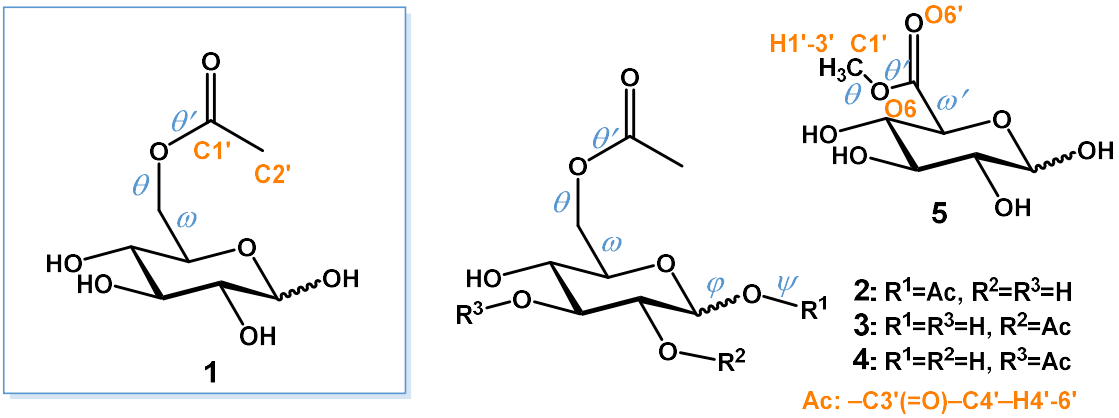

Figure 1. Model compound *α/ß*-**1** and the test set used for the development of a Karplus equation for the relationship between ^3J(Csp^2-O-C-H) coupling constants and the θ (C5-C6-O6-C1') dihedral angle.

It should be noted that while the current research was in progress, Turney *et al.*, published their investigation on the conformation of *O*-acetyl side chains in monosaccharides, which also produced a Karplus relationship for the aforementioned C(sp^2)OCH torsion, using a somewhat different method.[15] As will be discussed, their results corroborate our findings presented herein.

Results and Discussion

Synthesis

To study of the C(sp^2)OCH Karplus relationship on a simple carbohydrate ester model compound, we initially envisioned a simple regioselective acetylation of glucose to give 6- *O*acetyl-α/*ß*-D-glucopyranose **1**. A number of enzymatic and non-enzymatic methods for regioselective acetylation of unprotected or partially protected carbohydrates have been discussed in the literature.[16-19] Nevertheless, several attempts at regioselective acetylation using established non-enzymatic methods or adaptations thereof failed using unprotected glucose, despite their demonstrated success with methyl D-glucopyranoside.[18,20] The transformation was instead successful following a less direct synthetic route. Using a regioselective acetylation of per-TMS protected D-glucose **6** followed by selective deprotection of the silyl protection groups, **1** was obtained as a 42:58 mixture of *α*/*ß*-anomers.[21,22] In the regioselective acylation of per-TMS D-glucose **6** to give the monoacetylated **7**, en route to **1**, the reaction also yielded the diacetylated **8** in 16% yield. As described by Witschi *et al*., the DOWEX 50WX8-mediated deprotection of **7** and **8** proceeded with minimal acetyl migration to give a mixture of anomers of **1** and **2**, respectively.[22] In addition, the *α*/*ß*-**2** could be converted through acetyl migration into a mixture containing the more thermodynamically stable 2,6- (*α*/*ß*-**3**) and 3,6-isomers (*α*/*ß*-**4**) by heating of the diacetyl-glucose solution to 40 °C overnight. Their presence was verified *via* 1D TOCSY experiments which identified the hydrogens on the pyranose ring for *α*/*ß*-**3** and *α*/*ß*-**4** (see Methods section for the observed chemical shifts). In addition, a small amount of 6- *O*acetyl-D-glucose **1** was present in the mixture because of deacetylation. Meanwhile, no significant amounts of 4,6-di-*O*acetyl-D-glucose were observed by ^{1}H NMR. A fourth compound to be used in validating of the Karplus equation, the methyl ester of glucuronic acid **5**, was readily accessible from D-glucurono-6,3-lactone using methanol under basic conditions in 71% yield and was isolated as a 60:40 mixture of *α*/*ß*-anomers after separation from unreacted lactone by column chromatography.[23] The above synthesized compounds (or mixtures of isomers in the case of **3** and **4**) were analyzed by 1D and 2D NMR and full spectral assignments could be made. Compounds **1** and **5** were measured in D_2O, while **2** and the isomeric mixture containing **3** and **4** were measured in 2:1 D_2O:MeOD-d_4 due to their limited solubility in water alone. The addition of deuterated methanol was not expected to significantly affect the conformational behavior of the carbohydrates, due to the similar polarity of the solvents. The assignments of the synthesized compounds were corroborated by those published in the literature, where applicable.[19,22]

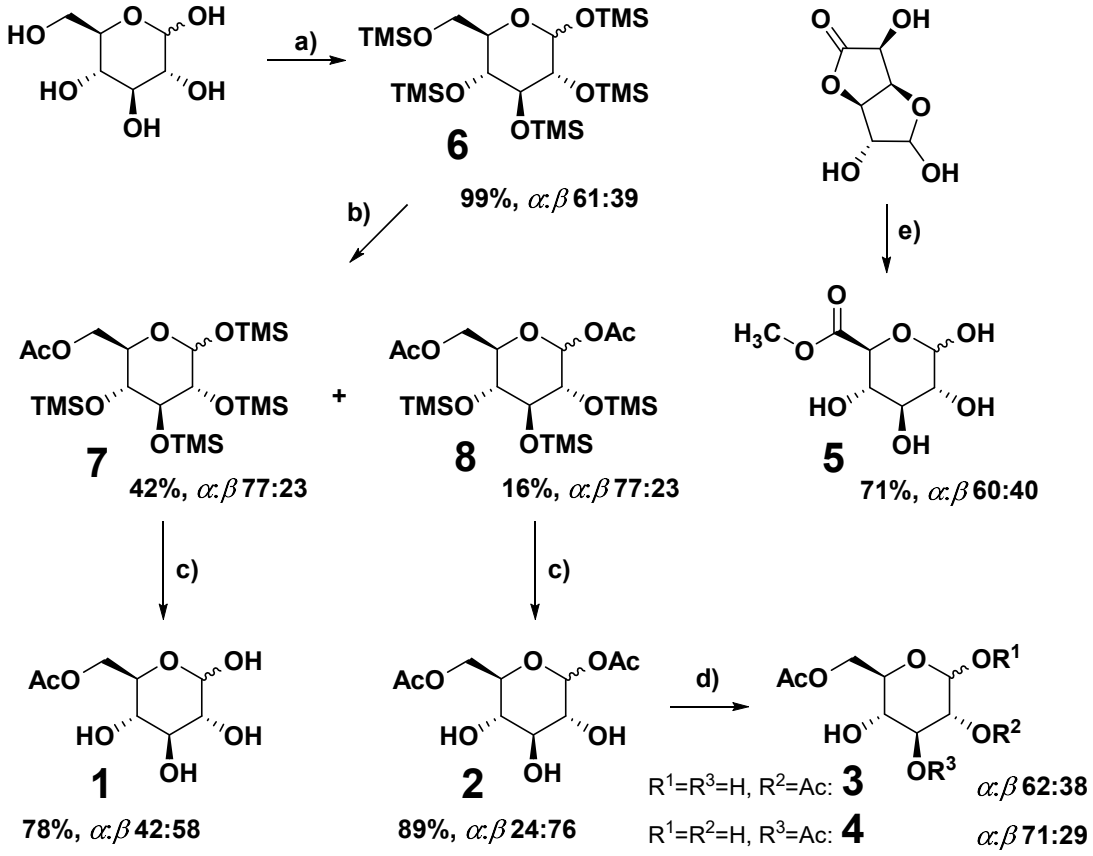

Figure 2. Scheme for the synthesis of model compounds *α/ß*-**1**, *α/ß*-**2**, *α/ß*-**3**, *α/ß*-**4** and *α/ß*-**5** used in this study. Conditions: a) HMDS, TMSOTf, CH_2Cl_2, rt, overnight; b) AcOH, Ac_2O, rt, 7 d; c) DOWEX 50WX8, MeOH, rt, 15 min; d) H_2O, MeOH, 40 °C, overnight; e) Na, MeOH, rt, 1 h.

Experimental determination of $^3J_{CH}$ coupling constants

Hetereonuclear three-bond couplings were measured using a gradient-selected *J*-HMBC experiment, as described by Willker and Leibfritz, that yielded pseudo-three dimensional HMBC spectra with the coupling evolution time τ on the z-axis.[24] An example of this is shown on page S10 in the Supplemental Information. Coupling constants were extracted for a given ^{1}H-^{13}C cross-peak in the HMBC spectrum based on the modulation of the peak volume (*A*) of the cross-peak as a function of τ in the *J*-HMBC spectra: *A* fluctuates in sinusoidal fashion with increasing coupling evolution time τ. In the experiment, *A* is measured as $|A|$ and thus every second lobe in the coupling evolution time slice was inverted to negative value, if applicable. The resulting data was fitted using PSI-Plot to a sinusoidal function of $A = B * \sin(\pi\, {}^3J_{CH} \cdot \tau)$, with B serving as a pre-factor for scaling to the arbitrary peak volume to yield the coupling constants for the relevant three bond couplings along the dihedral angles of interest with a precision uncertainty of about ±0.6 Hz.[24,25] The relevant $^3J_{Csp2OCH}$ coupling constants that were determined in this fashion are discussed hereafter and summarized in Table 3 and Table 5.

Molecular modeling

To establish a computational model for **1**, both molecular dynamics simulations and quantum mechanical calculations were performed. An exhaustive dihedral angle scan was performed on both *α*- and *ß*-anomers of

1 using Spartan14 to arrive at an initial guess for the lowest energy conformers of *α*/*ß*-**1**, as detailed in the Methods section. After this, the Amber14 software package and the carbohydrate-specific GLYCAM06 force field employing the TIP3P water model was used to run a 500 ns molecular dynamics simulation to sufficiently sample the conformational space of both *α*-**1** and *ß*-**1**.[26,27] The molecular dynamics treatment of the model compound was employed due to its known capability to characterize the internal molecular motion and flexible nature of carbohydrates.[1,28] The MD simulations were analyzed with respect to the population maxima of ω (C4-C5-C6-O6), θ (C5-C6-O6-C1') and θ' (C6-O6-C1'-C2') and 9 major conformational regions could be distinguished for both *α*-**1** and *ß*-**1** (sampling window ± 37°). The results are summarized in Table 1 and Table 2 and Figure 3 and 4). This captured 97% of the total 50000 conformers obtained for the two anomers, respectively.

Table 1. Summary of the conformational space of *α*-**1** established based on 97% of the total conformers based on 500ns MD simulation

α-**1** Conformer	C4-C5-C6-O6 ω / °	C5-C6-O6-C1' θ / °	C6-O6-C1'-C2' θ' / °	Count	% abundance
1	58	180	180	17759	37
2	58	103	180	5342	11
3	58	-106	180	4194	9
4	-73	180	180	4686	10
5	-73	103	180	2381	5
6	-73	-106	180	2189	4
7	-168	180	180	6370	13
8	-168	103	180	2774	6
9	-168	-106	180	2661	5
				48356	97% coverage

Table 2. Summary of the conformational space of *ß*-**1** established based on 97% of the total conformers based on 500ns MD simulation

ß-**1** Conformer	C4-C5-C6-O6 ω / °	C5-C6-O6-C1' θ / °	C6-O6-C1'-C2' θ' / °	Count	% abundance
1	58	180	180	18373	38
2	58	103	180	8049	17
3	58	-106	180	4280	9
4	-73	180	180	4053	8
5	-73	103	180	1755	4
6	-73	-106	180	1686	3
7	-168	180	180	5203	11
8	-168	103	180	1971	4
9	-168	-106	180	3035	6
				48575	97% coverage

In the case of both *α*-**1** and *ß*-**1**, conformer 1 (ω = 58°, θ = 180°, θ' = 180°) was the dominant conformational region at 37% and 38%, respectively. For *α*-**1**, ω largely favored g^+ (58°) with 57% abundance over the *st* (-168°) conformation at 24%, with the remainder of 19% present as g^- (-73°). The ω angle thus was predicted to behave similar to that of unsubstituted *α*-D-glucose, as described by Stenutz *et al*.[29,a] For θ, a 60% preference for the *st* (180°) conformation was predicted, while the g^+ (103°) and g^- (-106°) conformations contributed 22% and 18%, respectively. Meanwhile, the θ' angle was computed to entirely assume the *st* (180°) conformation due to the carbonyl on C1', which was supported by experimental evidence.[15] For *ß*-**1**, the ω angle assumed a slightly larger proportion of the g^+ conformation at 64%, over both the *st* and g^- conformations at 19% and 15%, thus differing slightly from unsubstituted *ß*-D-glucose which was assumed to

[a] Unpublished results from our laboratory corroborate these findings.

have a higher amount of *st*.[29] As a result, the second most abundant conformational region for *ß*-**1** was conformer 2 [ω = 58° (*g*$^+$), θ = 103° (*g*$^+$), θ' = 180° (*st*)] at 17% in *ß*-**1**, as opposed to conformer 7 [ω = –168° (*st*), θ = 180° (*st*), θ' = 180° (*st*)] at 13% in *α*-**1**. For θ, the dihedral angle population appeared largely unchanged between *α*-**1** and *ß*-**1**, with *ß*-**1** also displaying a large preference for the *st* conformation with 57%, and the *g*$^+$ and *g*$^-$ conformations contributing 25% and 18%, respectively. The broad distribution of θ in both *α*-**1** and *ß*-**1** – as seen in Figure 3 andFigure 4 – can very likely be attributed to little steric hindrance from neighboring positions, as also observed by Turney *et al*.[15] As was seen for *α*-**1**, the θ' angle in *ß*-**1** was entirely in the *st* conformation due to the carbonyl.

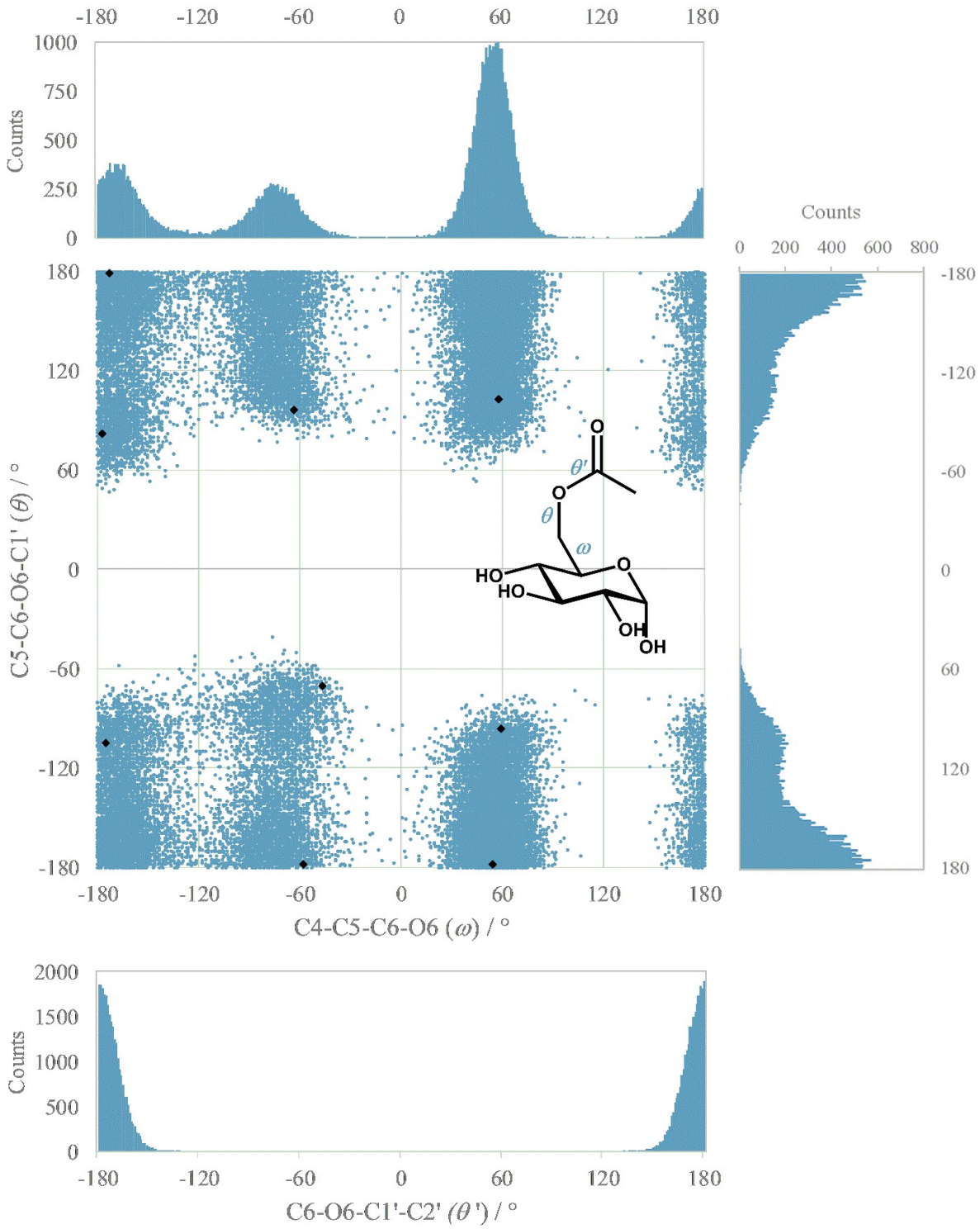

Figure 3. Summary of MD simulation for *α*-**1** showing population histograms and Ramachandran plot data for the relevant dihedral angles θ (C5-C6-O6-C1'), ω (C4-C5-C6-O6) and θ' (C6-O6-C1'-C2') – QM minimized conformers are overlaid as black diamonds to show their respective dihedral angle values.

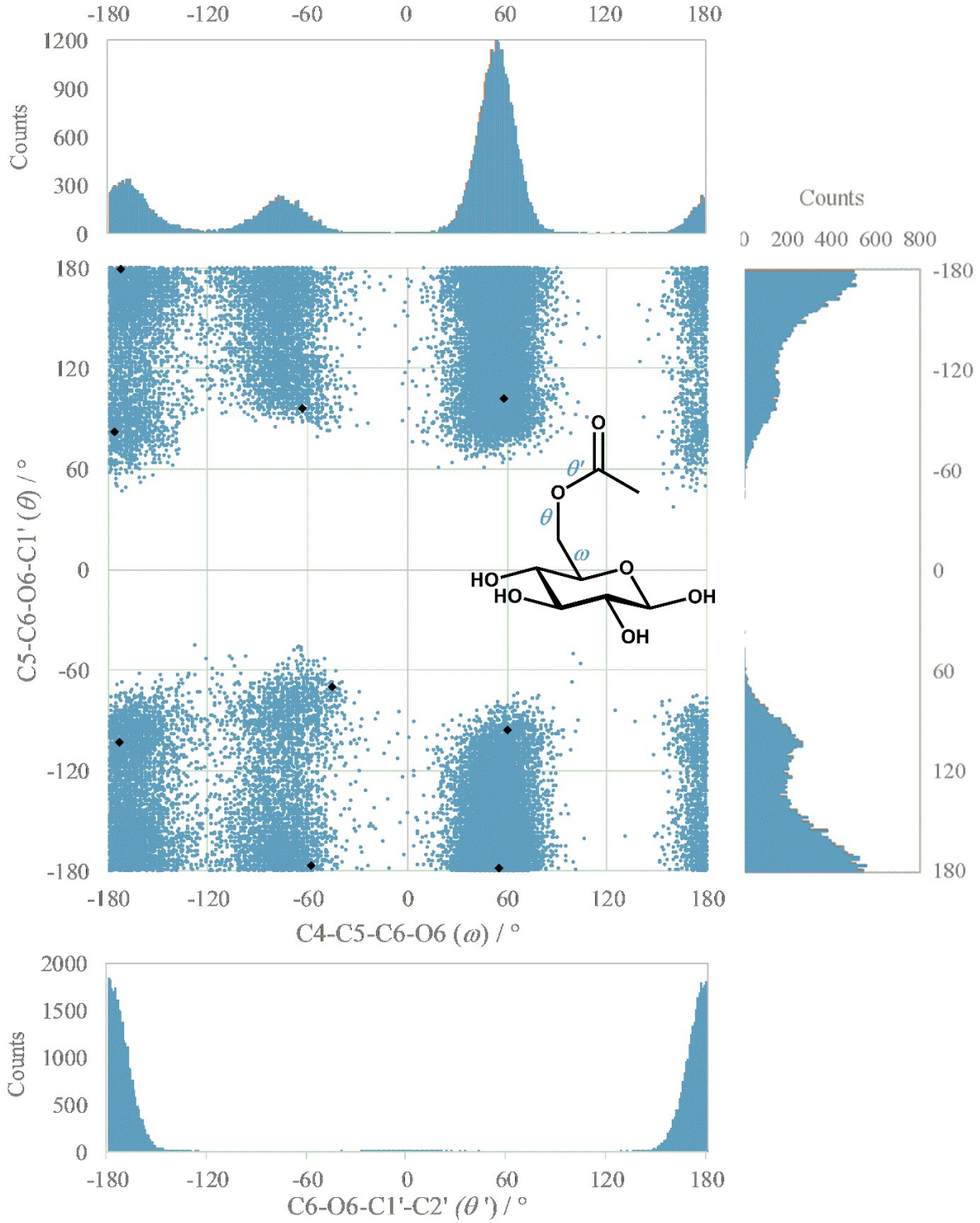

Figure 4. Summary of the MD simulation for *ß*-**1** showing population histograms and Ramachandran plot data for the relevant dihedral angles θ (C5-C6-O6-C1'), ω (C4-C5-C6-O6) and θ' (C6-O6-C1'-C2') – QM minimized conformers are overlaid as black diamonds to show their respective dihedral angle values.

With the conformational space of *α*-**1** and *ß*-**1** established, representative geometries for all 9 major conformers for both anomers were extracted from the MD trajectories and the geometries minimized using

Gaussian09 at the M05-2X/6-311+G**(PCM)//M05-2X/6-31G*(PCM) level of theory, as discussed in the Methods section. The θ and ω dihedral angle values for the minimized QM conformers are overlaid on the respective MD-derived Ramachandran plots in Figure 3 andFigure 4. Except for the cases of conformer region 6 (ω = –73°, θ = –106°, θ' = 180°), where the QM geometry shows a slight deviation in the ω angle from the mode of the MD simulation, they very closely matched the maxima of the dihedral angle populations, which supported the adequateness of the MD simulations. For each of the computed conformers, all other rotational minima around θ were computed. Based on the optimized geometries, relaxed geometry optimizations were then performed to compute the +/– 10°/20° rotated conformations, giving 270 molecular geometries total for each *α*-**1** and *ß*-**1**. This method, as opposed to a simple rotational scan of the dihedral angle at given angle increments, avoided placing undue emphasis on data from energetically unfavorable conformers, potentially skewing the Karplus fit. Specifically, the region between θ = –60° and θ = +60°, which was expected to be unpopulated on the basis of the MD simulations for *α*-**1** and *ß*-**1**, was omitted from impacting the fitting to a Karplus-type equation, in this way. Finally, Fermi contact value calculations were performed for all structures at the M05-2X/6-311G**[u+1s](PCM) level of theory to obtain values for the Fermi contact term for $^3J_{C1',H6R/S}$ in both *α*-**1** and *ß*-**1**. Only the Fermi contact term was considered based on findings from previous studies, as detailed in the Methods section.[30,31] The computed values were then plotted against the C5-C6-O6-C1' dihedral angle in accordance with the IUPAC convention for carbohydrate nomenclature. The resulting data points for (θ | $^3J_{C1',H6R}$) and (θ | $^3J_{C1',H6S}$) showed the expected Karplus-type relationship and, notably, as apparent from the relatively small spread of the data, data from all 9 conformers gave congruent results.

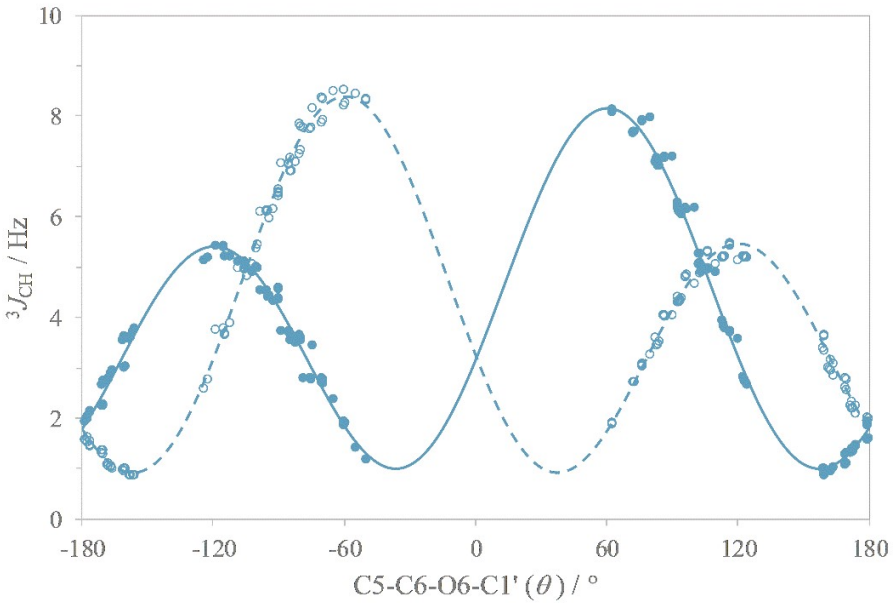

Figure 5. Computed coupling constants ^3J(C1'-H6$_R$) (solid circles and line) and ^3J(C1'-H6$_S$) (hollow circles and dashed line) for *α*/*ß*-**1** plotted against θ(C5-C6-O6-C1') overlaid with the Karplus equation fit.

This provides evidence for the small influence of the conformation away from θ and at the anomeric carbon on the coupling constants corresponding to the θ angle for *α*/*ß*-**1**. As such, the 9 conformers of each anomer were not weighed based on their relative abundance from the MD simulation or the relative energies from their QM optimization. Instead, their computed coupling constants for $^3J_{C1',H6R}$ and $^3J_{C1',H6S}$ could be fitted

to a four parameter Karplus equation of the form $^3J_{CH} = A \cdot \cos^2(\theta + B) + C \cdot \cos(\theta + B) + D$ (see Figure 5) for both anomers together to give the following two Karplus equations based on the C5-C6-O6-C1' dihedral angle:

$$^3J_{C1',H6_{proR}} = 5.69 \cdot \cos^2(\theta + 119.67°) - 1.37 \cdot \cos(\theta + 119.67°) + 1.09 \quad (1)$$

$r^2 = 0.996$, rms = 0.06

$$^3J_{C1',H6_{proS}} = 5.91 \cdot \cos^2(\theta - 120.29°) - 1.46 \cdot \cos(\theta - 120.29°) + 1.02 \quad (2)$$

$r^2 = 0.998$, rms = 0.11

As can be observed, the obtained coefficients are very similar for the two equations with the phase shift parameter *B* giving virtually the same absolute value. Because of this, the two sets of data could be combined by plotting the computed coupling constant values against the C1'-O6-C6-H6$_{R/S}$ dihedral angle θ^* to give a generalized three parameter Karplus equation for C(sp^2)-O-C-H dihedral angles:

$$^3J_{C-O-C-H} = 5.81 \cdot \cos^2\theta^* - 1.42 \cdot \cos\theta^* + 1.05 \quad (3)$$

$r^2 = 0.997$, rms = 0.12

As seen in Figure 6, the resulting three parameter Karplus equation bears close resemblance to that obtained by Turney *et al.*, which was fitted using a seven parameter equation.[15] Using the newly established Karplus equations (1) and (2), the MD simulations of *α/ß*-**1** were used to calculate predicted values for $^3J_{C1',H6R/S}$ from the θ dihedral angle distribution. As seen in Table 3, the computed coupling constants based on MD data are in excellent agreement with those from the *J*-HMBC experiment within the experimental error. The identity of the two hydrogens on C-6 were assigned unambiguously as H6$_R$ and H6$_S$ in both cases based on homonuclear three-bond coupling constants.

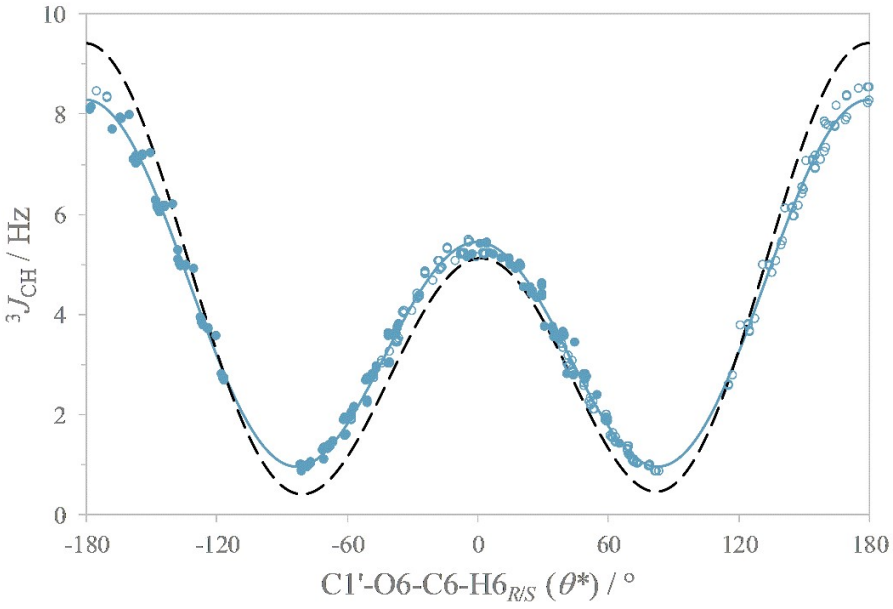

Figure 6. Overlay of fitted data for both ^3J(C1'-H6$_{R/S}$) plotted against the θ* (C1'-O6-C6-H6$_{R/S}$) angle and fitted Karplus equation (solid line), along with Karplus equation published by Turney *et al.* (dashed line).[15]

For this, the experimentally determined coupling constants were compared to theoretical values which were back calculated using published Karplus equations for $^3J_{H5,H6R/S}$ and $^2J_{H6R,H6S}$.[32] The resulting values do not compare as favorably to the experimentally determined coupling constants as the $^3J_{CH}$ values, but the magnitude of the $^3J_{HH}$ coupling constants is sufficiently different to allow for the distinction between H6$_R$ and H6$_S$. In the case of the $^3J_{HH}$ data, a slightly more satisfactory fit was obtained with a more specific Karplus equation. This is seen in the additional data included in parentheses for $^3J_{HH}$ in Table 3 calculated with Karplus equations parameterized on QM data for *α*/*ß*-D-glucose in our research group, although the magnitude of the $^3J_{H5,H6R}$ coupling was not fully captured.[b]

Table 3. Experimental *J*-HMBC, experimental HSQMBC [in brackets], and theoretical data for ^3J coupling constants of *α*/*ß*-**1**

	α-**1**		*ß*-**1**	
	exp.	MD[a]	exp.	MD[a]
$^3J_{C1',H6R}$	3.1 [3.6]	3.1 (2.8[15])	3.1 [3.2]	3.2 (2.8[15])
$^3J_{C1',H6S}$	2.8 [4.5]	3.0 (2.8[15])	2.9 [4.4]	3.2 (2.9[15])
$^3J_{H5,H6R}$	4.8	3.6[32] (3.5[b])	5.7	3.5[32] (3.4[b])
$^3J_{H5,H6S}$	2.4	3.1[32] (2.6[b])	2.1	2.8[32] (2.3[b])
$^2J_{H6R,H6S}$	12.0	-10.1[32]	12.3	-10.3[32]

a) Theoretical values are back calculated from MD simulations using Karplus equations (1) and (2) or literature equations, as annotated.[15,32] b) Calculated based on unpublished results from our lab for $^3J_{H5,H6R/S}$ based on data related to D-glucose and D-galactose obtained with the same method as described here for **1**.

To test the newly established Karplus equation, it was applied to the case of *α/ß*-**2**, *α/ß*-**3**, *α/ß*-**4** and *α/ß*-**5**. For this, the compounds were treated using the established molecular dynamics procedure as outlined above for **1**. For the MD simulation of **2** and **5**, additional dihedral angle parameters were needed to describe the ester-linkage on the anomeric carbon and uronate, respectively. This expansion of the GLYCAM06 force field was performed following the same method used by Kirschner *et al.* in the original GLYCAM06 publication on the basis of small model compounds and parameter substitution.[26] Further details are discussed in the Methods section and the parameters are supplied in the Supplemental Material. Additionally, atomic charges of *α/ß*-**2** and *α/ß*-**5** were derived based on the RESP two-step fitting procedure first published by Cornell *et al.,* as described in the Methods section.[33]

Table 4 summarizes the results of the MD simulations for *α/ß*-**2**, *α/ß*-**3** and *α/ß*-**4** with respect to the relevant dihedral angles. In *α/ß*-**2**, φ was defined as O5-C1-O1-C3' in accordance with IUPAC recommendations. By analogy, φ denotes the C1-C2-O2-C3' and C2-C3-C3-C3' dihedral angles in *α/ß*-**3** and *α/ß*-**4**, respectively. In Table 4, data for φ was summarized without assigning g^+/g^- or *st*, because of ambiguity in the definition of the respective dihedral angle. As can be seen, the θ, ω and θ' dihedral angles are unchanged from *α/ß*-**1**. The φ angle is more restrained than θ in all cases, due to the neighboring hydroxyl groups and the exo-anomeric effect. As illustrated in Figure 7, φ is least flexible in *α/ß*-**4** and *ß*-**3**, where the acetyl group is flanked by two equatorial hydroxyl groups on both sides, leading to a unimodal distribution. In *α/ß*-**2** and *α*-**3**, only one equatorial hydroxyl group results in a bimodal distribution around φ. In all compounds, ψ is constrained to the *st* conformation due to the carbonyl function, as already established for θ'.

Table 4. Summary of the relevant dihedral angle distributions for *α/ß*-**2**, *α/ß*-**3** and *α/ß*-**4** based on their MD simulations

Angle	Preference	*α*-**2**	*ß*-**2**	*α*-**3**	*ß*-**3**	*α*-**4**	*ß*-**4**
ω	g^+ / %	63	62	63	66	61	65
	g^- / %	15	15	16	15	18	16
	st / %	22	23	21	19	21	19
θ	g^+ / %	22	21	22	25	21	25
	g^- / %	18	19	17	18	19	18
	st / %	60	60	61	57	60	57
θ'	g^+ / %	-	-	-	-	-	-
	g^- / %	-	-	-	-	-	-
	st / %	100	100	100	100	100	100
φ	%	71 (84°) 29 (137°)	61 (-78°) 39 (-128°)	60 (83°) 40 (132°)	100 (118°)	100 (-115°)	100 (-115°)
ψ	g^+ / %	-	-	-	-	-	-
	g^- / %	-	-	-	-	-	-
	st / %	100	100	100	100	100	100

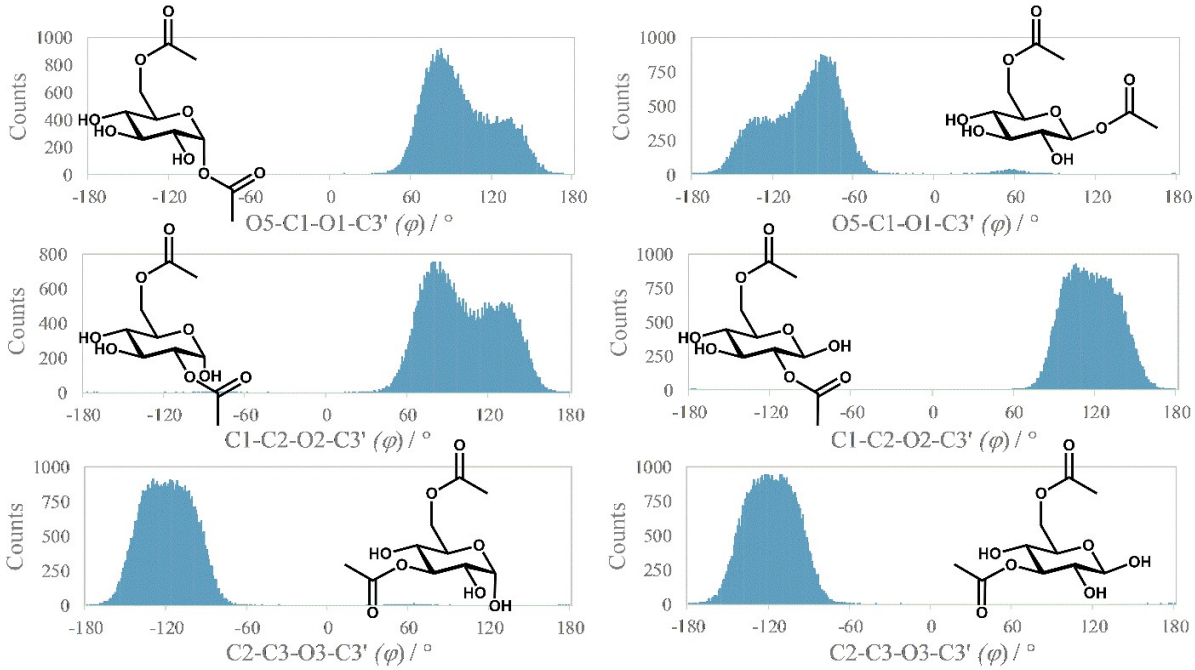

Figure 7. Summary of the φ dihedral angle for compounds *α*/*ß*-**2** (top), *α*/*ß*-**3** (middle) and *α*/*ß*-**4** (bottom row) showing the flexibility of the 1/2/3-acetyl linkage based on their MD simulations. Full conformational analysis for each compound in the Supplemental Material (Figures S3-S8).

The MD simulations of both *α*-**5** and *ß*-**5** displayed the expected high flexibility in the θ (C6-O6-C1'-H1') angle, with the dihedral population equally distributed between the maxima at g^+, g^- and *st*, because the methyl group attached to the carboxyl rotates freely. The θ' (C5-C6-O6-C1') angle was found to be constrained to ±180°, identical to *α*/*ß*-**1**. However, unlike the ω angle in the aforementioned model compound, ω' (C4-C5-C6-O6) in *α*-**5** and *ß*-**5** assumed only two maxima around –102° and +88°, roughly matching g^- and g^+ (*α*-**5**: 75% g^-, 25% g^+, *ß*-**5**: 76% g^-, 24% g^+). There is no preference for the *st* conformation, due to the carbonyl moiety of the ester group. This is comparable to the effect of the carboxylate group that also shows only two minima for this angle.[26] In the calculation of theoretical coupling constants for $^3J_{C6,Me\text{-}H}$ from *α*/*ß*-**5**, the contribution from all three protons in the methyl group was averaged, as is the case in the experimental observable.[13]

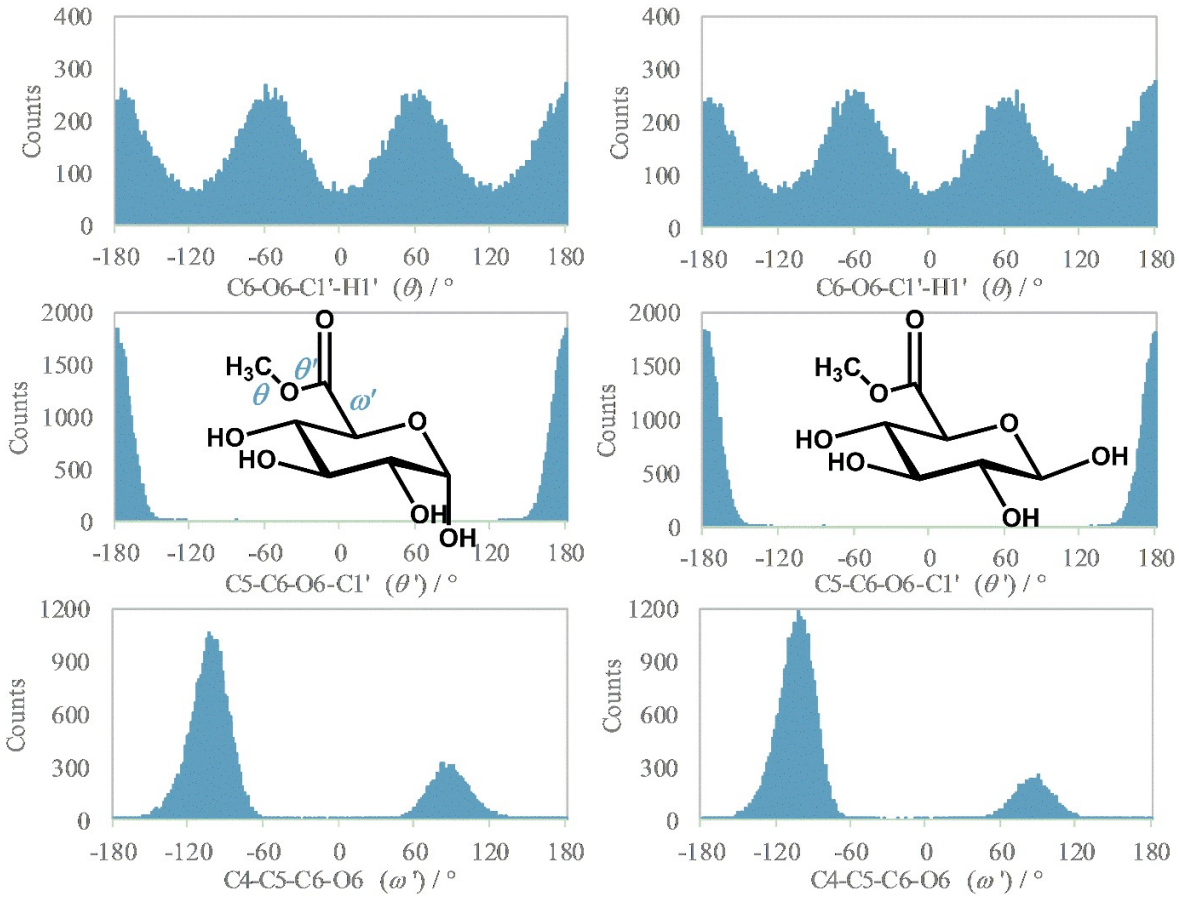

Figure 8. Histograms depicting the population distribution of the three relevant dihedral angles θ (C6-O6-C1'-H1'), θ' (C5-C6-O6-C1') and ω' (C4-C5-C6-O6) from the MD simulations of *α*-**5** (left) and *ß*-**5** (right).

As illustrated in Table 5, the experimental and back calculated theoretical $^{3}J_{CH}$ coupling constant data for the test set was generally in good agreement within range of the experimental error (about ±0.6 Hz). Notably, no experimentally relevant difference was observed between the seven-parameter equation by Turney *et al.* and the three-parameter equation presented herein.[15] The coupling constants determined for $^{3}J_{C1',H6R/S}$ in **2** - **4** were essentially unchanged from those in **1**, as was expected based on their MD simulations. The coupling constants determined from the MD simulations of *α*/*ß*-**2** and *α*/*ß*-**4** with equation (3) for the 1- and 3-acetyl linkage fall within the experimental error of the values determined from the *J*-HMBC experiment for *α*/*ß*-**2** and *α*/*ß*-**4**. In the case of the 2-acetyl linkage, a combined value was obtained for the $^{3}J_{C3',H2}$ correlation in *α*-**3** and *ß*-**3**, as their cross peaks overlap. The computationally derived coupling constant for *α*-**3** was comparable to the measured value, however the value determined for *ß*-**3** fell outside the range of the experimental error. This could be due to the overlap in the *J*-HMBC spectrum or the MD simulation being a less than perfect representation of the actual conformational behavior of *ß*-**3**. For *α*-**5** and *ß*-**5**, a satisfactory fit of the computational and experimental coupling constant for the methyl group could be obtained.

Table 5. Summary of experimental J-HMBC, experimental HSQMBC [in brackets], and theoretical (in parentheses) data for $^3J_{CH}$ coupling constants of *α*/*ß*-**2**, *α*/*ß*-**3,** *α*/*ß*-**4** and *α*/*ß*-**5**

exp. (MD)	*α*-**2**	*ß*-**2**	*α*-**3**	*ß*-**3**	*α*-**4**	*ß*-**4**	*α*-**5**	*ß*-**5**
$^3J_{C1',H6R}$	n.d.[a] [n.d.] (3.2,2.8)	3.0 [n.d.] (3.1,2.8)	3.1[b] [n.d.] (3.1,2.7)	3.2[b] [n.d.] (3.2,2.8)	3.1[b] [n.d.] (3.1,2.7)	3.2[b] [n.d.] (3.2,2.8)		
$^3J_{C1',H6S}$	2.6 [n.d.] (3.0,2.8)	2.6 [n.d.] (3.1,2.8)	2.8[b] [n.d.] (3.1,2.8)	3.0[b] [n.d.] (3.2,2.9)	2.8[b] [n.d.] (3.1,2.8)	3.0[b] [n.d.] (3.2,2.9)		
$^3J_{C3',H1}$	3.5 [n.d.] (4.0,3.5)	3.5 [n.d.] (4.2,3.8)						
$^3J_{C3',H2}$			3.6[c] [n.d.] (4.1,3.7)	3.6[c] [n.d.] (4.9,4.5)				
$^3J_{C3',H3}$					4.2 [n.d.] (3.5,3.6)	3.9 [n.d.] (3.6,3.7)		
$^3J_{C6,Me-H}$							3.9 [3.7] (4.0,3.9)	4.0 [4.4] (4.0,3.9)

Theoretical values are back calculated from MD simulations using Karplus equation (3) for $^3J_{C1',H6R/S}$ (left) and using the equation from Turney *et al*. (right).[15] a) no data due to spectral overlap for $^3J_{C1',H6S}$ correlation in *α*-**2**; b) determined from crosspeak overlap of *α*-**3** and *α*-**4**, due to spectral overlap; c) determined from crosspeak overlap of *α*-**3** and *ß*-**3**, due to spectral overlap.

One-bond ^{1}H-^{13}C-coupling values from non-decoupled HSQC-experiments vary by up to 4 Hz (determined in ^{1}H-dimension) and up to 7 Hz (determined in the ^{13}C-dimension) in the presence of strong ^{1}H-^{1}H-coupling.[34] To this end, we investigated whether three-bond ^{1}H-^{13}C-couplings in HMBC spectra of ester functional groups were similarly affected as has been cautioned in the literature.[35] Methods for the determination of long-range ^{1}H-^{13}C-couplings based on TOCSY-techniques[36,37] were not suitable because of the lack of attached protons at the ester carbonyl carbon. We chose the pure-shift in-phase/anti-phase (IPAP) HSQMBC experiment,[38,39] and reproduced previously published[37] ^{1}H-^{13}C-couplings from a menthol standard in $CDCl_3$ to within 0.7 Hz error (Supplemental Material). In addition, we performed NMR-spectral simulations to complement the results from HSQMBC and *J*-HMBC experiments.[24] The non-decoupled HMBC spectra of all compounds were simulated by solving the Liouville von-Neumann equation for the time-dependent behavior of coupled spin systems during an NMR pulse sequence. The experimental *J*-HMBC spectra yielding the coupling constants $^3J_{C1',H6R/S}$ were compared to the simulated spectra. One-bond coupling constants in the simulation were set to a typical value of 150 Hz. Whereas the simulated ^{1}H-spectrum (^{13}C-enriched spin system, single-pulse experiment) showed only negligible errors from the entered value, the simulated HMBC spectrum was characterized in all cases by spectral artifacts introduced presumably by cumulative errors in the multi-pulse sequence. In our hands, theoretical ^1J-values obtained from the purely simulated HMBC spectrum deviated by up to 1.2 Hz from the

entered value. On the other hand, theoretical ^{3}J-values only deviated by up to 0.5 Hz from the entered values, which was very similar to the error found in our experiments. Unfortunately, several coupling constants could not be determined by the HSQMBC experiment in our hands, presumably because of low sample concentration and low sensitivity of the HSQMBC experiment (Tables 3 & 5). Whereas experimental $^{3}J_{C1',H6R}$ couplings of α-**1** and β-**1** were similar to the *J*-HMBC results, the corresponding $^{3}J_{C1',H6S}$ values were markedly different (Table 3). The HSQMBC $^{3}J_{C6,Me\text{-}H}$ couplings in α/β-**5** were identical within experimental error to those determined by *J*-HMBC (Table 5).

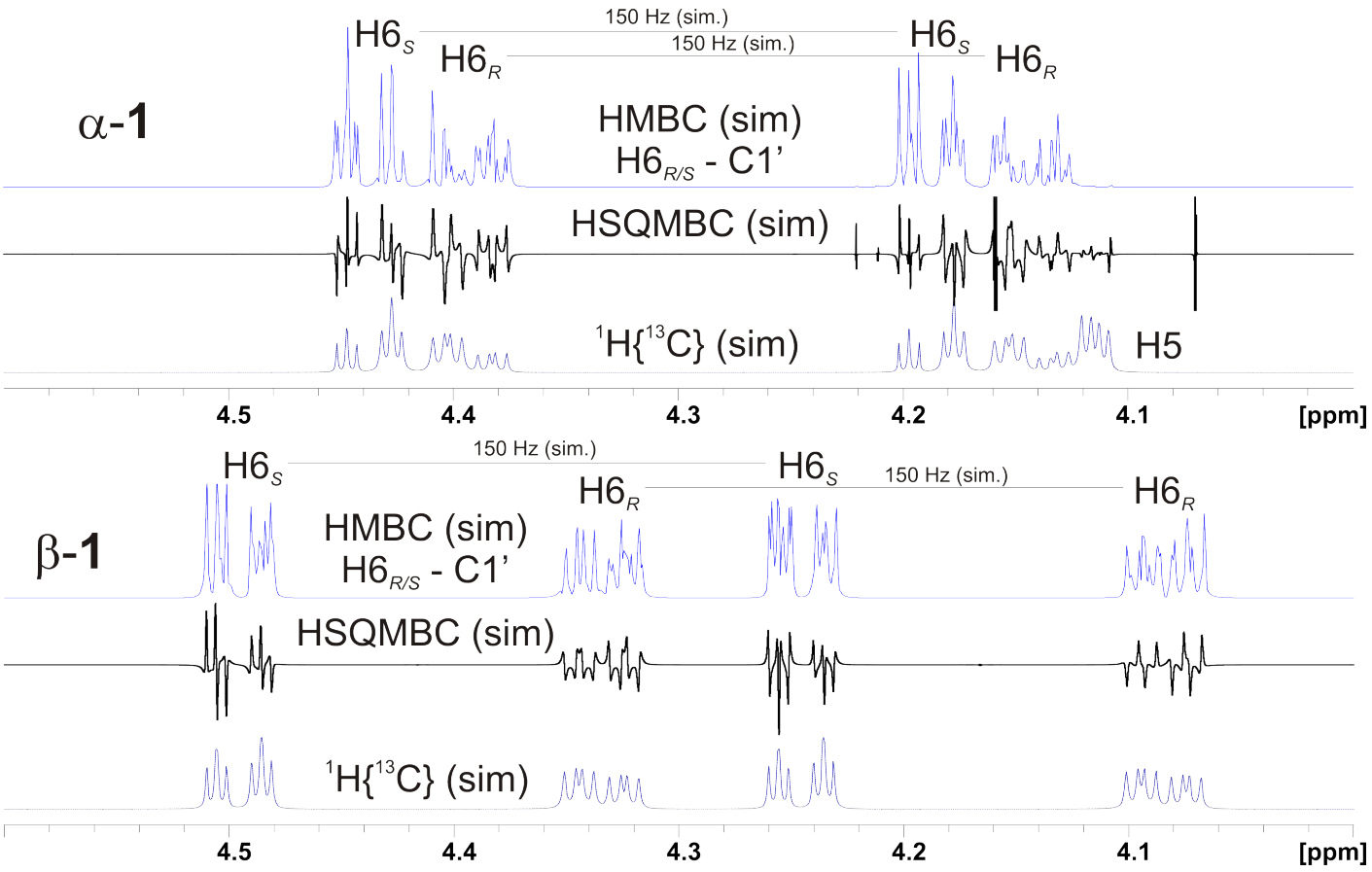

Figure 9. Simulation of purely theoretical NMR-spectra (top trace: non-decoupled qf-HMBC; bottom trace: coupled ^{1}H-spectrum with ^{13}C-enrichment) of α-**1** and β-**1**. The ^{1}H-projection of the HMBC spectrum is along the C1' chemical shift at 174.14 ppm for α-**1** and at 174.17 ppm for β-**1**. Coupling constants for α-**1** and β-**1** were: $^{1}J_{H,C}$ = 150 Hz and $^{2}J_{H,C}$ = -5 Hz as typical values. All three-bond *J*-values were set to experimental values determined by us via the *J*-HMBC experiment (see Experimental and Supplemental Material).

Overall, the close fit between experimental *J*-HMBC and theoretical coupling constant data for the C(sp^2)-O-C-H coupling pathway in the test compounds supported the premise that both the newly established Karplus equation and the MD simulations presented herein are good approximations of the true relationships and conformational behavior of the studied compounds. The Karplus equation should thus be applicable to other ester-linked carbohydrates, cautiously considering the potentially different conformational behavior of configurational isomers, including equatorial and axial substitution and possible ring puckering, that needs to be accounted for in the modeling of the compounds of interest. In addition, it is possible that, as described by others,[34] and as observed by us in HSQMBC experiments, coupling pathways between other pairs of nuclei, *e.g.*, strongly-coupled protons such as H6$_{R/S}$ and H5, influence the $^{3}J_{H,C(sp2)}$-value, possibly experiment-

dependent, and require consideration in the construction of a more accurate Karplus equation. In the present study and because of the limited number of compounds investigated, we were unable to satisfactorily interpret the observed difference in coupling constants determined by *J*-HMBC and HSQMBC experiments.

Conclusions

A Karplus equation for the C(sp^2)-O-C-H coupling pathway in ester-linked carbohydrates was developed based on quantum mechanical and molecular mechanics computations for 6-acetyl-*α*/*ß*-D-glucopyranose **1**. The obtained Karplus relationship was validated with a carbohydrate-based test set of esters represented by acetyl groups on positions 1, 2, 3 and 6 of a carbohydrate moiety, as well as glucuronic acid methyl ester. In addition, the presented results expand the application of the GLYCAM06 force field to uronate esters and anomeric esters. The presented data support that a combination of computational (MD simulations using a carbohydrate specific force field and NMR spectral simulations) and experimental data (NMR data from *J*-HMBC/IPAP-HSQMBC experiments) can be used to establish the conformational space of ester-linked carbohydrates using the Karplus equations established herein. Deviations in magnitude between a few long-range ^{1}H-^{13}C-couplings determined by *J*-HMBC or HSQMBC were observed. Because of the limited number of compounds studied, it was not possible to conclude if the deviation was due to strong ^{1}H-^{1}H-couplings.

Experimental Section

General. All reagents were obtained from Sigma-Aldrich and used without further purification, unless otherwise indicated. Solvents were distilled prior to use. Column chromatography was performed on silica gel (Sorbent Technologies, 40-75 μm) and fractions analyzed with TLC run on equivalent mobile phase, or as noted, and visualized through charring with 10% H_2SO_4/MeOH solution. ^{1}H and ^{13}C NMR spectra were acquired on a JEOL ECA-600 NMR-spectrometer (600 and 150 MHz, respectively). Structural assignments were corroborated by homo- and heteronuclear 2D NMR methods (COSY, HMQC, HMBC and TOCSY) where necessary. Accurate mass measurements were performed on a JEOL AccuTOF Mass Spectrometer (Peabody, MA, USA) equipped with an ESI source with polyethyleneglycol as an internal calibrant. NMR analyses and ESI-HRMS spectra of the characterized compounds are included in the Supplemental Material.

Synthetic methods

Trimethylsilyl 2,3,4,6-tetra-trimetylsilyl-α/ß-D-glucopyranose 6. Scaled up from the literature.[21] In a 2-neck flask flushed with N_2, placed glucose (2.02 g, 11.2 mmol) and then added dichloromethane (20 mL), hexamethyldisilazane (7.5 mL, 35.8 mmol, 3.2 equiv) and TMSOTf (400 μL, 2.2 mmol, 0.2 equiv) to give a white suspension. Stirred under N_2 overnight, after which it was a clear colorless solution. Evaporated solvent with reduced pressure and redissolved in hexane (50 mL). Washed with DI water (3 × 12 mL). Extracted aqueous layers with hexane (10 mL), then washed the combined organic layers with brine (30 mL), then dried with sodium sulfate. After filtration and evaporation, a clear colorless liquid (6.04 g, 99%, *α:ß* 61:39) was obtained and used without further purification. R_f (9:1 hex:EtOAc) 0.85. ^{1}H NMR (600 MHz, $CDCl_3$): δ 5.00 (d, 3.0 Hz, *α*-1), 4.45 (d, 7.2 Hz, *ß*-1), 3.77 (t, 9.0 Hz, 1H), 3.75-3.64 (m, 2H-*α*, 1H-*ß*), 3.60 (dd, 6.0 Hz, 10.8 Hz, *ß*), 3.44-3.37 (m, 1H-*α*, 2H-*ß*), 3.33 (dd, 3.0 Hz, 9.0 Hz, *α*-2), 3.24-3.19 (m, 2H, *ß*), 0.16 (s, 9H, *α*-Si$(CH_3)_3$), 0.16 (s, 9H, *ß*-Si$(CH_3)_3$), 0.15 (s, 9H, *α*-Si$(CH_3)_3$), 0.15 (s, 9H, *ß*-Si$(CH_3)_3$), 0.14 (s, 9H, *ß*-Si$(CH_3)_3$), 0.14 (s, 9H, *α*-Si$(CH_3)_3$), 0.14 (s,

9H, *ß*-Si(CH_3)$_3$), 0.12 (s, 9H, *α*-Si(CH_3)$_3$), 0.10 (s, 9H, *α*-Si(CH_3)$_3$), 0.10 (s, 9H, *ß*-Si(CH_3)$_3$). ^{13}C NMR (150 MHz, $CDCl_3$): δ 98.24 (*ß*-1), 93.97 (*α*-1), 78.51 (*ß*), 77.61 (*ß*), 76.97 (*ß*), 74.26 (*α*), 74.10 (*ß*), 72.53 (*α*), 72.35 (*α*), 72.05 (*α*), 62.40 (*α*), 62.38 (*ß*), 1.47 (*ß*), 1.42 (*ß*), 1.36 (*α*), 1.05 (*α*), 1.02 (*ß*), 0.55 (*α*), 0.53 (*α*), 0.27 (*α*), -0.15 (*ß*), -0.37 (*ß*). HRMS (DART-MS): *m/z* calculated for $C_{21}H_{52}O_6Si_5$ $[M]^{\bullet+}$ 540.2610, found 540.2862; *m/z* calculated for $C_{15}H_{33}O_4Si_3$ $[M - 2 \times TMS\text{-}OH]^{\bullet+}$ 361.1681, found 361.1650. All analytical data matched those previously reported.[21]

Trimethylsilyl 6-acetyl-2,3,4-tris-trimethylsilyl-α/ß-D-glucopyranoside 7 and **acetyl 6-acetyl-2,3,4-tris-trimethylsilyl-α/ß-D-glucopyranoside 8**. Based on literature preparation. [22] In a 100 mL round bottom flask, placed per-TMS-D-glucose (1.194 mg, 2.2 mmol) and added pyridine (4.3 mL), acetic anhydride (3.2 mL) and acetic acid (273 µL, 2.2 equiv). Stirred the clear solution for 7 days at room temperature to give a clear slightly yellow reaction mixture. Diluted with dichloromethane (100 mL) and washed with 0.5 M HCl solution (2 × 150 mL), back extracting the combined aqueous layers with dichloromethane (25 mL). After washing with sat. Na_2CO_3 solution (100 mL), dried organic layers over Na_2SO_4. After filtration, evaporated solvent to yield a colorless clear oil which was separated via column chromatography (95:5 → 9:1 hexane:ethyl acetate) to yield tetramethylsilyl 6-acetyl-2,3,4-tetramethylsilyl-α/ß-D-glucose (0.47 g, 42%) and acetyl 6-acetyl-2,3,4-tetramethylsilyl-α/ß-D-glucose (0.17 g, 16%). *Trimethylsilyl 6-acetyl-2,3,4-tris-trimethylsilyl-α/ß-D-glucopyranoside* **7**: clear colorless oil. R_f (9:1 hex:EtOAc) 0.59/0.49. α:ß 77:23. ^{1}H NMR (600 MHz, $CDCl_3$): δ 5.02 (d, 3.0 Hz, *α*-1), 4.46 (d, 7.8 Hz, *ß-1*), 4.34 (dd, 1.5 Hz, 11.7 Hz, *ß-6a*), 4.30 (dd, 2.4 Hz, 12.0 Hz, *α*-6a), 4.06 (dd, 4.8 Hz, 12.0 Hz, *α*-6b), 4.00 (ddd, 1.8 Hz, 4.8 Hz, 12.0 Hz, *ß-6b*), 3.91 (ddd, 2.4 Hz, 4.8 Hz, 9.6 Hz, *α*-5), 3.79 (app. t, 9.0 Hz, *α*-3), 3.45 (app. t, 9.0 Hz, *α*-4), 3.41-3.38 (m, 3H, *ß-5,4,3)*, 3.37 (dd, 3.0 Hz, 9.6 Hz, *α*-2), 2.09 (s, 3 H, *α*-Ac), 2.06 (s, 3H, *ß*-Ac), 0.16 (s, 9 H, *ß*-TMS), 0.16 (s, 9 H, *α*-TMS), 0.16 (s, 9 H, *ß*-TMS), 0.15 (s, 9 H, *α*-TMS), 0.14 (s, 9 H, *α*-TMS), 0.14 (s, 9 H, *ß*-TMS), 0.13 (s, 2 x 9 H, *α*-TMS + *ß*-TMS). ^{13}C NMR (150 MHz, CDCl3): δ 171.1 (*α)*, 94.1 (*α)*, 74.1 (*α)*, 74.0 (*α)*, 72.5 (*α)*, 70.0 (*α)*, 64.0 (*α)*, 21.1 (*α)*, 1.4 (*α)*, 1.0 (*α)*, 0.6 (*α)*, 0.2 (*α)*. HRMS (DART-MS): *m/z* calculated for $C_{20}H_{50}NO_7Si_4$ $[M + NH_4]^+$ 528.2664, found 528.2854. *Acetyl 6-acetyl-2,3,4-tris-trimethylsilyl-α/ß-D-glucopyranoside* **8**: clear colorless oil. R_f (9:1 hex:EtOAc) 0.29/0.24. α:ß 77:23. ^{1}H NMR (600 MHz, $CDCl_3$): *δ* 6.08 (d, 3.6 Hz, *α*-1), 5.43 (d, 7.2 Hz, *ß*-1), 4.34 (dd, 2.4 Hz, 12.0 Hz, *ß*-6a), 4.32 (dd, 2.4 Hz, 12.0 Hz, *α*-6a), 4.04 (dd, 5.4 Hz, 12.0 Hz, *α*-6b), 4.02 (dd, 5.4 Hz, 12.0 Hz, *ß*-6b), 3.81 (ddd, 2.4 Hz, 4.8 Hz, 10.2 Hz, *α*-5), 3.74 (app. t, 9.0 Hz, *α*-3), 3.57 (dd, 3.0 Hz, 9.0 Hz, *α*-2), 3.53 (m, 2H, *α*-4, *ß*-5), 3.45 (m, 3H, *ß*-2, *ß*-3, *ß*-4), 2.12 (s, 3H, *ß*-Ac), 2.10 (s, 3 H, *α*-Ac), 2.08 (s, 3 H, *α*-Ac), 2.07 (s, 3 H, *ß*-Ac), 0.16 (s, 9 H, *ß*-TMS), 0.16 (s, 9 H, *α*-TMS), 0.16 (s, 9 H, *α*-TMS), 0.15 (s, 18 H, 2 × *ß*-TMS), 0.12 (s, 9 H, *α*-TMS). ^{13}C NMR (150 MHz, $CDCl_3$): *δ* 170.9, 170.9, 169.6, 169.3, 94.5, 92.2, 78.1, 74.9, 74.7, 74.1, 72.4, 72.3, 71.7, 71.6, 63.5, 63.3, 21.2, 20.8, 20.7, 1.1, 1.0, 0.8, 0.7, 0.7, 0.0. HRMS (DART-MS): *m/z* calculated for $C_{19}H_{44}NO_8Si_3$ $[M + NH_4]^+$ 498.2375, found 498.2520. All analytical data matched those previously reported. [22]

6-*O*-Acetyl-α/ß-D-glucopyranose 1. Adapted from the literature. [22] To the TMS-derivate **7** (85 mg, 0.17 mmol) in a round bottom flask flushed with nitrogen was added dry methanol (3 mL) and DOWEX 50WX8 resin (0.50 g) and stirred at rt. After 10 min, TLC showed **7** to be fully consumed. The reaction mixture was then filtered at 15 min and evaporated. The obtained yellow to orange clear oil was dried under high vacuum overnight (29 mg, 0.13 mmol, 78%). α:ß 42:58. ^{1}H NMR (600 MHz, $CDCl_3$): *δ* 5.18 (d, 4.2 Hz, *α*-1), 4.62 (d, 7.8 Hz, *ß*-1), 4.37 (dd, 2.1 Hz, 12.3 Hz, *ß*-6$_S$), 4.31 (dd, 2.4 Hz, 12.0 Hz, *α*-6$_S$), 4.27 (dd, 4.8 Hz, 12.0 Hz, *α*-6$_R$), 4.21 (dd, 5.7 Hz, 12.3 Hz, *ß*-6$_R$), 3.99 (ddd, 2.4 Hz, 4.5 Hz, 10.2 Hz, *α*-5), 3.68 (t, 9.6 Hz, *α*-3), 3.63 (ddd, 2.4 Hz, 4.8 Hz, 9.9 Hz, *ß*-5), 3.50 (dd, 3.9 Hz, 9.9 Hz, *α*-2), 3.47-3.41 (m, *α*-4, *ß*-4, *ß*-3), 3.22 (apt t, 9.0 Hz, *ß*-2), 2.09 (s, *ß*-CH_3), 2.09 (s, *α*-CH_3). ^{13}C NMR (150 MHz, $CDCl_3$): *δ 174.17, 174.14, 96.04 (ß-1), 92.18 (α-1), 75.54, 74.02 (ß-2), 73.36 (ß-5), 72.60 (α-3), 71.41 (α-2), 69.60, 69.52, 69.12 (α-5), 63.49 (2C, α-6, ß-6), 20.23, 20.21.* HRMS (ESI-MS): *m/z* calculated for $C_8H_{14}O_7Na$ $[M + Na]^+$ 245.0637, found 245.0653.

Acetyl 6-*O*-acetyl-α/ß-D-glucopyranoside 2. Adapted from the literature. [22] To the TMS-derivate **8** (90.8 mg, 0.19 mmol) in a round bottom flask flushed with nitrogen was added 3 mL dry methanol and DOWEX 50WX8 resin (0.50 g) and stirred at rt. After 10 min, TLC showed **8** to be fully consumed and the reaction mixture was filtered and evaporated. The obtained yellow to orange clear oil was dried under high vacuum overnight (45.2 mg, 0.17 mmol, 89%). *α*:*ß* 24:76. ^{1}H NMR (600 MHz, $CDCl_3$): *δ* 6.03 (d, 3.6 Hz, *α*-1), 5.48 (d, 8.4 Hz, *ß*-1), 4.35 (dd, 2.1 Hz, 12.3 Hz, *ß*-6$_S$), 4.29 (dd, 2.4 Hz, 12.0 Hz, *α*-6$_S$), 4.22 (dd, 4.8 Hz, 12.0 Hz, *α*-6$_R$), 4.21 (dd, 5.6 Hz, 12.0 Hz, *ß*-6$_R$), 3.87 (ddd, 2.4 Hz, 5.6 Hz, 10.2 Hz, *α*-5), 3.71 (t, 9.6 Hz, *α*-3), 3.70 (ddd, 2.4 Hz, 4.8 Hz, 9.9 Hz, *ß*-5), 3.65 (dd, 3.9 Hz, 9.9 Hz, *α*-2), 3.51 (t, 9.9 Hz, *ß*-3), 3.45 (t, 9.6 Hz, *α*-4), 3.43 (t, 9.6 Hz, *ß*-4), 3.41 (t, 9.6 Hz, *ß*-2), 2.16 (s, *α*-CH_3).2.15 (s, *ß*-CH_3), 2.07 (s, *α*-CH_3), 2.07 (s, *ß*-CH_3). ^{13}C NMR (150 MHz, $CDCl_3$): *δ 174.98 (C=O, α-6Ac), 174.95 (C=O, ß-1-Ac), 173.75 (C=O, α-1-Ac), 173.42 (C=O, ß-1-Ac), 95.29 (ß-1), 93.29 (α-1), 76.72 (ß-3), 75.62 (ß-5), 74.09 (α-3), 73.28 (ß-2), 72.92 (α-5), 71.49 (α-2), 70.59 (ß-4), 70.55 (α-4), 64.55 (α-6), 64.36 (ß-6), 21.49, 21.49, 21.33, 21.33.* HRMS (DART-MS): *m/z* calculated for $C_{10}H_{16}O_8Na$ $[M + Na]^+$ 287.0743, found 287.0709.

Mixture containing 2,6-di-*O*-acetyl-α/ß-D-glucopyranose 3 and **3,6-di-*O*-acetyl-α/ß-D-glucopyranose 4**. Heating of a solution of **2** (25 mg) in D_2O:MeOD-d_4 (0.6 mL, 2:1 by volume) to 40 °C for 14 h overnight induced acetyl migration to form a mixture containing *ß*-**2** (due to the slower acetyl migration from *ß*-**2** compared to *α*-**2**), *α*-**3**, *ß*-**3**, *α*-**4**, *ß*-**4** and *α*-**1**, *ß*-**1**, as determined by 1D-TOCSY experiments (see Supplemental Material for spectra and assignments). The ratio of the compounds was determined by ^{1}H NMR to be 1:0.48:0.30:0.32:0.13:0.17:0.37, respectively.

Methyl α/ß-D-glucopyranuronate 5. Adapted from the literature. [23] In a flame-dried round bottom flask, added D-glucurono-6,3-lactone (0.688 g, 3.90 mmol), dry methanol (4 mL) and a small piece of sodium. The suspension was stirred at room temperature for 4 h to yield an orange-amber clear solution. After evaporation to give an orange sticky syrup, NMR showed 84% conversion to the desired methyl ester. The product was isolated using column chromatography (100% ethyl acetate, dry loading) to give the desired product as colorless crystals (0.581 g, 2.8 mmol, 71%). R_f (EtOAc) 0.2. *α:ß* 60:40. ^{1}H NMR (600 MHz, $CDCl_3$): δ 5.26 (d, 3.6 Hz, *α*-1), 4.69 (d, 8.4 Hz, *ß*-1), 4.38 (d, 10.2 Hz, *ß* -5), 4.07 (d, 9.6 Hz, *α*-5), 3.81 (s, *α*-CH_3), 3.81 (s, *ß*-CH_3), 3.73 (t, 9.3 Hz, *α*-3), 3.60-3.55 (m, 3H, *α*-2, *α*-4, *ß*-4), 3.51 (t, 9.3 Hz, *ß*-3), 3.29 (apt t, 8.7 Hz, *ß*-2). ^{13}C NMR (150 MHz, CDCl3): δ 171.99 (*ß*-C=O), 171.05 (*α*-C=O), 96.20 (*ß*-1), 92.44 (*α*-1), 75.13 (*ß*-3), 74.64 (*α*-5), 73.68 (*ß*-2), 72.30 (*α*-3), 71.48, 71.28, 71.05, 70.66 (*ß*-5), 53.10 (CH_3), 53.07 (CH_3). HRMS (DART-MS): *m/z* calculated for $C_7H_{12}O_7Na$ $[M + Na]^+$ 231.0481, found 231.0501.

NMR methods. Samples were prepared with concentrations between 0.1-0.5 M in the appropriate solvent as specified above. All 1D-spectra were recorded at rt with sample spinning (15 Hz) on an JEOL ECA-600 NMR spectrometer unless specifically stated. Standard NMR tubes with OD 5mm (600 MHz quality) were used. The ^{1}H- and ^{13}C-spectra were zero-filled 4 times prior to Fourier transformation. Except for ^{1}H-^{1}H-COSY, all 2D-spectra and experiments were recorded without sample spinning. 2D spectra were zero-filled 4 times in the 1H dimension and 2 times in the ^{13}C dimension prior to Fourier transformation.

Three-bond heteronuclear coupling constants were determined using a gradient-selected HMBC experiment, as described by Willker and Leibfritz, [24] with 8 scans over a 1638 × 512 data point matrix with an incrementally increasing coupling evolution time of τ = 0-260 ms (in 20 ms increments) and a relaxation delay of 3s. Composite 180°-pulses were used to minimize error propagation from dephasing of magnetization during the multi-pulse sequence. The FID was modulated using a 1.0 Hz Gaussian window function in the ^{1}H dimension and a sinebell function (shift -10°, size 110) in the ^{13}C dimension and zero filled twice in either dimension prior to Fourier transformation. The resulting data related to the modulation of the cross-peak

volume of the three-bond ^{1}H-^{13}C correlations of interest were fitted to A = B * sin($\pi \cdot {}^{3}J_{CH} \cdot \tau$) using PSI-Plot to yield the coupling constants for the relevant three bond $^{3}J_{CH}$ couplings, as illustrated in the Supplemental Information on page S10. [25] Complementary IPAP-HSQMBC experiments were carried out. Data for a menthol standard (30 wt% in $CDCl_3$) was collected in 4 scans (rt, no spinning) without zero-filling. All other samples were analyzed with 32 scans (rt, no spinning), 4k data points in the ^{1}H-dimension, 256 data points in the ^{13}C-dimension, and optimized spectral windows within 11-13 h each.

Computational methods

Conformer search. The initial conformer searches for compounds **1**, **2**, **3**, **4** and **5** (both anomers, respectively) were performed using the Spartan14 software suite. [40,41] The input geometry was restrained to the preferred chair conformation, with twist and boat conformations excluded. The conformer distribution was computed using MAXCYCLES = 1000 and MAXCONFORMERS = 20000 with 100% conformers kept at the HF/6-31G*//AM1 level of theory (implicit solvent model used). The lowest energy conformer fitting the above criteria was chosen as the starting geometry for the molecular dynamics computations.

Molecular dynamics. Molecular dynamics simulations of both anomers of **1**, **2**, **3**, **4** and **5** were run using the Amber14 software suite and the GLYCAM06 force field, which has been specially parameterized to the flexible behavior of carbohydrate molecules.[26,42] Input files were generated on the basis of .pdb files from Spartan14 conformer search using the format taken from the Glycam webtool Carbohydrate Builder.[43] Simulations were performed using explicitly modeled solvent environment with the TIP3P water model and periodic boundary conditions of 8 Å. Minimization and heating were both performed using a commonly used two-step procedure, with the initial minimization and heating step, respectively, affecting only solvent molecules by using positional restraints on the carbohydrate molecule. The production runs were performed over 500 ns to sufficiently sample the available conformational space. [26,27] The MD simulation input parameters are also supplied in the Supplemental Material. All MD runs were monitored for successful equilibration prior to and stability during the production run based on energy and pressure data extracted using the existing process_mdout.perl and process_minout.perl scripts. Extraction of dihedral angle values using vmd from the MD trajectories was preceded by editing of the .prmtop and .mdcrd files to remove water molecules using the CPPTRAJ utility.

Parameter expansion for the GLYCAM06 force field. The GLYCAM06 force filed was expanded to include torsion parameter terms for Os-Cg-Os-C and H2-Cg-Os-C for the 1-acetyl linkage in **2** and Os-Cg-C –O , Os-C –Cg-Os and Os-C Cg-H1 to parameterize the 6-ester-linkage and allow for the use of the Carbohydrate specific force field use with methyl *α*/*ß*-D-glucopyranuronate **5**. The 1-acetyl linkage could be modeled using substitutions with existing parameters for Cg-Cg-Os-C and H1-Cg-Os-C, respectively. This resulted in a mean error of 1.15 kcal/mol or 14.8% of the highest rotational barrier compared to QM calculations for a test set of *α*/*ß*-**2** and tetrahydropyran-2-yl acetate, which was considered sufficient on the basis of similar errors in the original GLYCAM06 publication. [26] Detailed results can be found in the Supplemental Material. The procedure for the parametrization of the 6-ester-linkage was adapted from the GLYCAM06 publication and used two model compounds, namely methyl methoxyacetate and methyl tetrahydropyran-2-acetate. The necessary Molecular Mechanics computations were performed using Amber14 over 2000 cycles of steepest descent algorithm, followed by up to 4000 cycles following the conjugate gradient algorithm – using dihedral angle constraints to obtain the same geometry as in the DFT calculations. Related input files and results of the parameter fitting are replicated in the Supplemental Material, together with the developed torsion parameters. The resulting systemic mean error of 0.37 kcal/mol compared to QM calculations compares favorably to that obtained for the carboxylate functional group in the original GLYCAM06 paper. [26]

Atomic charge generation. The atomic charges supplied with GLYCAM06 were adjusted for **1**, **3** and **4** based on established procedures to account for the acetyl group derivation by modifying the charge of the bonded glycan carbon by +0.008. [44] In the absence of preexisting atomic charges for acetyl 6-acetyl-*α*/*ß*-D-glucopyranoside **2** and methyl *α*/*ß*-D-glucopyranuronate **5** in the GLYCAM06 force field parameters, they were derived using the two-stage RESP fit protocol, as established by Cornell *et al.* [33] After an initial RESP fit based on Gaussian esp calculations (using the undocumented iop(6/33=2) option and pop=chelpg) and the espgen and respgen utilities of AmberTools16, a 50 ns MD simulation was run with the initial atomic charges. [42] Then, 100 representative geometries were extracted from the MD trajectory and optimized at the HF/6-31G* level of theory, followed by a second RESP fit as described above which was averaged across all 100 conformers to give final values for the atomic charges for both anomers of **2** and **5**, respectively. The Gaussian input files were prepared using a modified version of a python script described by Reisbick and Willoughby. [45]

Quantum mechanical calculations*.* Computations were performed using the Gaussian09 software package. [46] Geometries were optimized at the M05-2X/6-31G* level of theory using tight optimization criteria on ultrafine integration grid and used implicit PCM solvent correction for water. The M05-2X Minnesota functional was chosen for this study, as it was found by Csonka *et al.* and others to give better energetics for carbohydrates than the commonly used B3LYP functional, provided a higher density DFT grid was used. [47-49] Additionally, Bally *et al.* found that reoptimization of geometry optimizations performed using the 6-31G* basis set with larger basis sets generally changed calculated coupling constants very little (rms change below 0.15 Hz) and if the 'mixed' option is invoked, geometry reoptimization had even less of an effect. [30] The inclusion of diffuse functions (+) did not give notably better results, but increases time requirement more than 3-fold. Thus, 6-31G* was chosen as the basis set for the current study as a good compromise between accuracy and computational expense. In their study, Bally *et al.* also found no improvement upon adding implicit solvent model, however as this might not be the case with water and carbohydrates, implicit PCM solvent correction was included. [30] The xyz coordinates of the optimized geometries of all 9 conformers for both *α*-**1** and *ß*-**1** are supplied in the Supplemental Material. Torsional angle scans were performed using relaxed geometry scans using the above optimization criteria to obtain +/- 10/20° isomers. Fermi contact value calculations were performed using GIAO-NMR calculations (FConly, mixed) at the M052X/6-311G**[u+1s] level of theory and implicit PCM solvent correction for water. The larger basis set was modified to include polarization orbitals, but no diffuse functions, as Bally *et al*. found them not to add additional value in NMR calculations, while the increased valence functions improved rms error (6-311G(d,p) vs 6-31G(d,p)) at little additional computational cost. [30] The use of 'FCOnly' calculates only the Fermi contact term, saving significant computation time over the 'spinspin' option. As others have found, this is often the preferred option because the spin−orbit terms are negligible or cancel out for $^{3}J_{CH}$, thus leaving the Fermi contact term as the only relevant contribution. [30,31]

NMR simulations. The NMRSim 6.0 module in Bruker's TopSpin 3.5 pl7 software was used. Spin systems were defined by chemical shifts and by ^{1}H-^{1}H-/^{1}H-^{13}C-coupling constants for one-, two-, and three-bond couplings. Values for $^{1}J_{H,C}$ and $^{2}J_{H,C}$ were set at typical values of 150 Hz and -5 Hz, respectively. All other *J*-values were used as experimentally determined. Therefore, the CH-CH_2-O-C system for the ester linkage had three ^{1}H-shifts, three ^{13}C-shifts, three $^{1}J_{H,C}$-values (150 Hz), two $^{2}J_{H,C}$-values (- 5 Hz), two $^{3}J_{H,C}$-values (exp.), and two $^{3}J_{H,H}$-values (exp.). All spectra were simulated at 600.00 MHz (^{1}H) and 150.87 MHz (^{13}C). Fully-coupled ^{1}H-spectra of ^{13}C-enriched spin systems: The Bruker zg single-pulse sequence was used and 4 transients were simulated. The raw simulation (32k data points) was Fourier transformed. Non-decoupled ^{1}H-^{13}C-qf-HMBC spectra: The Bruker hmbcgplpndqf pulse sequence was used (AQ_mod = qsim, FnMODE = qf, SW = 2.0 pp, line broadening 0.5 Hz) and 4 transients were simulated followed by 4k zero-filling in both dimensions. HSQMBC spectra: The

Bruker hsqcetgplrsp pulse sequence was used (AQ_mod = qsim, FnMODE = Echo-Antiecho, SW = 2.0 pp, line broadening 0.5 Hz) followed by 4k zero-filling in both dimensions.

Acknowledgements

The authors thank the GLYCAM user group for insightful help and discussion on the expansion of the GLYCAM06 force field torsion parameters. We express thanks to Dr. Ashok Krishnaswami (JEOL, Inc.) for the compilation of the IPAP-HSQMBC experiment. This work used the Extreme Science and Engineering Discovery Environment (XSEDE), which is supported by National Science Foundation grant number ACI-1053575 (XSEDE Startup Allocation CHE 160038). [50]

Supplementary Material

Four-parameter version of the reported Karplus equation; preliminary data on tetrahydropyran-2-methyl acetate; NMR (^{1}H, ^{13}C) and HRMS data of all characterized compounds; molecular dynamics parameters and initial geometries; GLYCAM parameter fitting results; RESP derived atomic charges for **2** and **3**; graphical summary of conformational analyses; geometries of QM optimized conformers for **1**. NMR-simulations (NMRSim 6.0, Bruker).

References

1. Widmalm, G. *Carbohydr Res* **2013**, *378*, 123-132. http://dx.doi.org/10.1016/j.carres.2013.02.005.
2. Widmalm, G. In *Comprehensive Glycoscience*; J. P. Kamerling, Ed.; Elsevier: Oxford, 2007; Vol. 2, p 101-132.
3. Mazzanti, A.; Casarini, D. *Wiley Interdiscip. Rev.: Comput. Mol. Sci.* **2012**, *2*, 613-641. http://dx.doi.org/10.1002/wcms.96.
4. Frank, M. In *Bioinformatics for Glycobiology and Glycomics*; John Wiley & Sons Ltd.: Chichester, UK, 2009; p 337-357.
5. Grachev, A. A.; Gerbst, A. G.; Shashkov, A. S.; Nifantiev, N. E. *Russ. Chem. Rev.* **2009**, *78*, 717-736. http://dx.doi.org/10.1070/RC2009v078n08ABEH004061.
6. Karplus, M. *J. Am. Chem. Soc.* **1963**, *85*, 2870-2871. http://dx.doi.org/10.1021/ja00901a059.
7. Karplus, M.; Anderson, D. H.; Farrar, T. C.; Gutowsky, H. S. *J. Chem. Phys.* **1957**, *27*, 597-598. http://dx.doi.org/10.1063/1.1743784.
8. Ramsey, N. F. *Phys. Rev.* **1953**, *91*, 303-307. http://dx.doi.org/10.1103/PhysRev.91.303.
9. Toukach, F. V.; Ananikov, V. P. *Chem. Soc. Rev.* **2013**, *42*, 8376-8415. http://dx.doi.org/10.1039/c3cs60073d.
10. Coxon, B. In *Advances in Carbohydrate Chemistry and Biochemistry*; Academic Press: 2009; Vol. 62, p 17-82.
11. Minch, M. J. *Concepts Magn. Reson.* **1994**, *6*, 41-56. http://dx.doi.org/10.1002/cmr.1820060104.
12. Altona, C. In *Encyclopedia of NMR*; John Wiley & Sons, Ltd: 2007.

13. Grimmer, C. D.; Slabber, C. A. *Magn. Reson. Chem.* **2015**, *53*, 590-595. http://dx.doi.org/10.1002/mrc.4264.
14. González-Outeiriño, J.; Nasser, R.; Anderson, J. E. *J. Org. Chem.* **2005**, *70*, 2486-2493. http://dx.doi.org/10.1021/jo048295c.
15. Turney, T.; Pan, Q.; Sernau, L.; Carmichael, I.; Zhang, W.; Wang, X.; Woods, R. J.; Serianni, A. S. *J. Phys. Chem. B* **2017**, *121*, 66-77. http://dx.doi.org/10.1021/acs.jpcb.6b10028.
16. Kennedy, J. F.; Kumar, H.; Panesar, P. S.; Marwaha, S. S.; Goyal, R.; Parmar, A.; Kaur, S. *J. Chem. Technol. Biotechnol.* **2006**, *81*, 866-876. http://dx.doi.org/10.1002/jctb.1473.
17. Therisod, M.; Klibanov, A. M. *J. Am. Chem. Soc.* **1986**, *108*, 5638-5640. http://dx.doi.org/10.1021/ja00278a053.
18. Adinolfi, M.; Barone, G.; Iadonisi, A.; Schiattarella, M. *Tetrahedron Lett.* **2003**, *44*, 4661-4663. http://dx.doi.org/10.1016/S0040-4039(03)01072-4.
19. Brecker, L.; Mahut, M.; Schwarz, A.; Nidetzky, B. *Magn. Reson. Chem.* **2009**, *47*, 328-332. http://dx.doi.org/10.1002/mrc.2395.
20. Ishihara, K.; Kurihara, H.; Yamamoto, H. *J. Org. Chem.* **1993**, *58*, 3791-3793. http://dx.doi.org/10.1021/jo00067a005.
21. Joseph, A. A.; Verma, V. P.; Liu, X.-Y.; Wu, C.-H.; Dhurandhare, V. M.; Wang, C.-C. *Eur. J. Org. Chem.* **2012**, *2012*, 744-753. http://dx.doi.org/10.1002/ejoc.201101267.
22. Witschi, M. A.; Gervay-Hague, J. *Org. Lett.* **2010**, *12*, 4312-4315. http://dx.doi.org/10.1021/ol101751d.
23. Bollenback, G. N.; Long, J. W.; Benjamin, D. G.; Lindquist, J. A. *J. Am. Chem. Soc.* **1955**, *77*, 3310-3315. http://dx.doi.org/10.1021/ja01617a047.
24. Willker, W.; Leibfritz, D. *Magn. Reson. Chem.* **1995**, *33*, 632-638. http://dx.doi.org/10.1002/mrc.1260330804.
25. Poly Software International Inc., PSI-Plot, 8.02a; Pearl River, NY, 2005
26. Kirschner, K. N., Yongye, A.B., Tschampel, S.M., Daniels, C.R., Foley, B.L, Woods, R.J. *J. Comput. Chem.* **2008**, *29*, 622-655. http://dx.doi.org/10.1002/jcc.20820.
27. Seo, M.; Castillo, N.; Ganzynkowicz, R.; Daniels, C. R.; Woods, R. J.; Lowary, T. L.; Roy, P.-N. *J. Chem. Theory Comput.* **2008**, *4*, 184-191. http://dx.doi.org/10.1021/ct700284r.
28. Pereira, C. S.; Kony, D.; Baron, R.; Muller, M.; van Gunsteren, W. F.; Hunenberger, P. H. *Biophys. J.* **2006**, *90*, 4337-4344. http://dx.doi.org/10.1529/biophysj.106.081539.
29. Stenutz, R.; Carmichael, I.; Widmalm, G.; Serianni, A. S. *J. Org. Chem.* **2002**, *67*, 949-958. http://dx.doi.org/10.1021/jo010985i.
30. Bally, T.; Rablen, P. R. *The J. Org. Chem.* **2011**, *76*, 4818-4830. http://dx.doi.org/10.1021/jo200513q.
31. Bagno, A.; Rastrelli, F.; Saielli, G. *J. Phys. Chem. A* **2003**, *107*, 9964-9973. http://dx.doi.org/10.1021/jp0353284.
32. Tafazzoli, M.; Ghiasi, M. *Carbohydr. Res.* **2007**, *342*, 2086-2096. http://dx.doi.org/10.1016/j.carres.2007.05.032.
33. Cornell, W. D.; Cieplak, P.; Bayly, C. I.; Kollmann, P. A. *J. Am. Chem. Soc.* **1993**, *115*, 9620-9631. http://dx.doi.org/10.1021/ja00074a030.
34. Yu, B.; van Ingen, H.; Vivekanandan, S.; Rademacher, C.; Norris, S. E.; Freedberg, D. I. *J. Magn. Reson.* **2012**, *215*, 10-22. http://dx.doi.org/10.1016/j.jmr.2011.09.037.
35. Bax, A.; Freeman, R. *J. Am. Chem. Soc.* **1982**, *104*, 1099-100. http://dx.doi.org/10.1021/ja00368a033.

36. Nolis, P.; Gil, S.; Espinosa, J. F.; Parella, T. *Magn. Reson. Chem.* **2009**, *47*, 121-132. http://dx.doi.org/10.1002/mrc.2363.
37. Vidal, P.; Esturau, N.; Parella, T.; Espinosa, J. F. *J. Org. Chem.* **2007**, *72*, 3166-3170. http://dx.doi.org/10.1021/jo0621120.
38. Gil, S.; Espinosa, J. F.; Parella, T. *J. Magn. Reson.* **2010**, *207*, 312-321. http://dx.doi.org/10.1016/j.jmr.2010.09.017.
39. Gil, S.; Espinosa, J. F.; Parella, T. *J. Magn. Reson.* **2011**, *213*, 145-150. http://dx.doi.org/10.1016/j.jmr.2011.09.036.
40. Wavefunction Inc., Spartan'14, Irvine, CA,
41. Shao, Y.; Molnar, L. F.; Jung, Y.; Kussmann, J.; Ochsenfeld, C.; Brown, S. T.; Gilbert, A. T. B.; Slipchenko, L. V.; Levchenko, S. V.; O'Neill, D. P.; DiStasio Jr, R. A.; Lochan, R. C.; Wang, T.; Beran, G. J. O.; Besley, N. A.; Herbert, J. M.; Yeh Lin, C.; Van Voorhis, T.; Hung Chien, S.; Sodt, A.; Steele, R. P.; Rassolov, V. A.; Maslen, P. E.; Korambath, P. P.; Adamson, R. D.; Austin, B.; Baker, J.; Byrd, E. F. C.; Dachsel, H.; Doerksen, R. J.; Dreuw, A.; Dunietz, B. D.; Dutoi, A. D.; Furlani, T. R.; Gwaltney, S. R.; Heyden, A.; Hirata, S.; Hsu, C.-P.; Kedziora, G.; Khalliulin, R. Z.; Klunzinger, P.; Lee, A. M.; Lee, M. S.; Liang, W.; Lotan, I.; Nair, N.; Peters, B.; Proynov, E. I.; Pieniazek, P. A.; Min Rhee, Y.; Ritchie, J.; Rosta, E.; David Sherrill, C.; Simmonett, A. C.; Subotnik, J. E.; Lee Woodcock Iii, H.; Zhang, W.; Bell, A. T.; Chakraborty, A. K.; Chipman, D. M.; Keil, F. J.; Warshel, A.; Hehre, W. J.; Schaefer Iii, H. F.; Kong, J.; Krylov, A. I.; Gill, P. M. W.; Head-Gordon, M. *Phys. Chem. Chem. Phys.* **2006**, *8*, 3172-3191. http://dx.doi.org/10.1039/B517914A.
42. Case, D. A. B., R.M; Botello-Smith, W.; Cerutti, D.S.; Cheatham III, T.E.; Darden, T.A.; Duke, R.E.; Giese, T.J.; Gohlke, H.; Goetz, A.W.; Homeyer, N.; Izadi, S.; Janowski, P.; Kaus, J.; Kovalenko, A.; Lee, T.S.; LeGrand, S.; Li, P.; Lin, C.; Luchko, T.; Luo, R.; Madej, B.; Mermelstein, D.; Merz, K.M.; Monard, G.; Nguyen, H.; Nguyen, H.T.; Omelyan, I.; Onufriev, A.; Roe, D.R.; Roitberg, A.; Sagui, C.; Simmerling, C.L.; Swails, J.; Walker, R.C.; Wang, J.; Wolf, R.M.; Wu, X.; Xiao, L.; York D.M. and Kollman P.A., AMBER 2016, University of California, San Francisco, 2016
43. Woods Group (2005-2016), *GLYCAM Web. Carbohydrate Builder.*, Complex Carbohydrate Research Center, University of Georgia, Athens, GA (http://glycam.org)
44. Foley, L. *Adding chemical derivatives to GLYCAM residues*, R. J. Woods, Ed., 2016 http://glycam.org/docs/help/2014/04/04/adding-chemical-derivatives-to-glycam-residues/
45. Reisbick, S.; Willoughby, P. *Protocol Exchange* **2014**, http://dx.doi.org/10.1038/protex.2014.015.
46. Frisch, M. J.; Trucks, G. W.; Schlegel, H. B.; Scuseria, G. E.; Robb, M. A.; Cheeseman, J. R.; Scalmani, G.; Barone, V.; Mennucci, B.; Petersson, G. A.; Nakatsuji, H.; Caricato, M.; Li, X.; Hratchian, H. P.; Izmaylov, A. F.; Bloino, J.; Zheng, G.; Sonnenberg, J. L.; Hada, M.; Ehara, M.; Toyota, K.; Fukuda, R.; Hasegawa, J.; Ishida, M.; Nakajima, T.; Honda, Y.; Kitao, O.; Nakai, H.; Vreven, T.; Montgomery Jr., J. A.; Peralta, J. E.; Ogliaro, F.; Bearpark, M. J.; Heyd, J.; Brothers, E. N.; Kudin, K. N.; Staroverov, V. N.; Kobayashi, R.; Normand, J.; Raghavachari, K.; Rendell, A. P.; Burant, J. C.; Iyengar, S. S.; Tomasi, J.; Cossi, M.; Rega, N.; Millam, N. J.; Klene, M.; Knox, J. E.; Cross, J. B.; Bakken, V.; Adamo, C.; Jaramillo, J.; Gomperts, R.; Stratmann, R. E.; Yazyev, O.; Austin, A. J.; Cammi, R.; Pomelli, C.; Ochterski, J. W.; Martin, R. L.; Morokuma, K.; Zakrzewski, V. G.; Voth, G. A.; Salvador, P.; Dannenberg, J. J.; Dapprich, S.; Daniels, A. D.; Farkas, Ö.; Foresman, J. B.; Ortiz, J. V.; Cioslowski, J.; Fox, D. J., Gaussian 09, Gaussian, Inc., Wallingford, CT, USA, 2009
47. Zhao, Y.; Schultz, N. E.; Truhlar, D. G. *J. Chem. Theory Comput.* **2006**, *2*, 364-382. http://dx.doi.org/10.1021/ct0502763.
48. Csonka, G. I.; French, A. D.; Johnson, G. P.; Stortz, C. A. *J. Chem. Theory Comput.* **2009**, *5*, 679-692. http://dx.doi.org/10.1021/ct8004479.
49. Marianski, M.; Supady, A.; Ingram, T.; Schneider, M.; Baldauf, C. *J. Chem. Theory Comput.* **2016**, *12*, 6157-6168.

http://dx.doi.org/10.1021/acs.jctc.6b00876.

50. Towns, J. C., T.; Dahan, M.; Foster, I.; Gaither, K.; Grimshaw, A.; Hazlewood, V.; Lathrop, S.; Lifka, D.; Peterson, G.D.; Roskies, R.; Scott, J.R.; Wilkins-Diehr, N. *Comput. Sci. Eng.* **2014**, *26*, 62-74. http://dx.doi.org/10.1109/MCSE.2014.80

